Calculating Trajectories for Atoms in
Near-resonant Lightfields*

R. E. Scholten, T. J. O'Kane, T. R. Mackin, T. A. Hunt and P. M. Farrell[A]

School of Physics, University of Melbourne,
Parkville, Vic. 3052, Australia.
[A]Optical Technology Research Laboratory, Victoria University,
Footscray, Vic. 3011, Australia.

Abstract

We review several methods for calculating the time development of the internal state and the external motion of atoms in near-resonant light fields, with emphasis on studying the focussing of atomic beams into microscopic and potentially nanoscopic patterns. Three different approaches are considered: two-level semiclassical, multi-level semiclassical, and the Monte Carlo wavefunction method. The two-level semiclassical technique of McClelland and Scheinfein (1991) and McClelland (1995) is extended to three dimensions, and used to calculate the trajectories of atoms and the imaging properties of a simple lens formed from a near-resonant travelling TEM_{01} mode laser. The model is then extended to multi-level atoms, where we calculate the density matrix for the internal state of a sample of thermal atoms in a standing wave, and show how cooling processes can be simulated. Finally, we use the Monte Carlo wavefunction method to calculate the internal state of the atom, and compare the results and required computation time to those of the multi-level semiclassical technique.

1. Introduction

The field of atom optics, in which atoms are manipulated in a similar fashion to the way light is controlled with conventional optics, has exploded in recent years. This development has been motivated by several advantages over classical light optics, neutron optics, and charged-particle optics (Adams *et al.* 1994). For example, atom optics is not bound by the Liouiville theorem, allowing cooling and trapping of atoms; thermal atoms have short de Broglie wavelengths which allows focussing to sub-nanometre scales; atoms are relatively heavy and therefore potentially sensitive to gravitational fields, and so on.

We are exploiting the short de Broglie wavelength of thermal atoms to manipulate them on microscopic and nanoscopic scales. In particular, we are exploring the potential for focussing a neutral atomic beam into arbitrary patterns only a few microns across, using near-resonant light.

The basic principle of using near-resonant laser light to focus atoms into nanometre scale patterns has been demonstrated experimentally. Chromium atoms have been focussed by a standing wave as they were evaporatively deposited onto a silicon substrate, forming a closely spaced array of parallel lines approximately

10.1071/PH99014   0004-9506/99/030493$10.00

60 nm in width (see Fig. 1) (McClelland *et al.* 1993, 1996; Scholten *et al.* 1994; Celotta *et al.* 1996). Other atoms have also been used (McGowan *et al.* 1995; Timp *et al.* 1992), and two-dimensional focussing has been used to form spots (Gupta *et al.* 1995) and hexagonal structures (Drodofsky *et al.* 1997*a*), but there has been little progress beyond these simple patterns. To form more complex and potentially arbitrary patterns we must create appropriate three-dimensional light fields. In designing the required field, there are many degrees of freedom, including the spatial distribution, intensity, frequency and polarisation of the light field. It is therefore essential that we are able to predict the atomic trajectories through an arbitrary field.
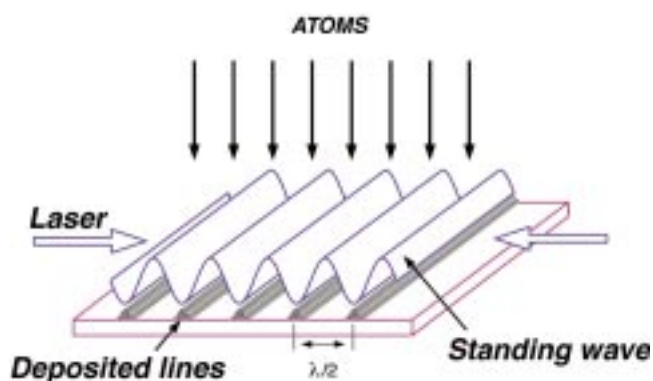
Fig. 1.   Atoms are focussed into the nodes of a standing wave detuned above resonance (McClelland *et al.* 1993).

In this paper, we explore several methods for calculating the temporal evolution of the internal state, and the external motion, of atoms in near-resonant light fields. Three different approaches are considered, all based on solving the fundamental quantum master equation. They extend from a two-level semiclassical model, to a multi-level semiclassical model based on solving the quantum master equation written in a form similar to the optical Bloch equations, and finally to the Monte Carlo wavefunction method.

The two-level semiclassical technique is used to calculate the trajectories of atoms in a lens formed by two near-resonant travelling TEM_{01} mode laser beams. This method has been used in two dimensions for standing waves (McClelland *et al.* 1993; McClelland and Scheinfein, 1991; McClelland, 1995), but we extend it to three dimensions so that the imaging properties of such lenses can be evaluated.

Using the optical Bloch equations we calculate the density matrix for the internal state of a sample of multi-level thermal atoms in a polarisation gradient standing wave. Using the density matrix we calculate the force on the atoms as for the two-level semiclassical method, and hence the trajectories of atoms during one dimensional laser cooling.

Finally, we demonstrate the utility of the Monte Carlo wavefunction method for calculating the internal state of the atom. Monte Carlo methods have been used for calculating trajectories and simulating laser cooling, but no detailed optical pumping calculations have been published for multi-level atoms. We compare

the Monte Carlo and Bloch equation methods, showing that Monte Carlo is at a significant disadvantage in computation time for problems with a small number of basis states.

2. Master Equation

The interactions between atoms and laser fields lie at the heart of problems ranging from spectroscopy (Demtröder 1981) to the theory of the gas laser (Lamb 1964), in addition to atom optics and laser cooling (Cohen-Tannoudji 1990; Ungar *et al.* 1989). For travelling waves, the calculation of the effect of these interactions on the internal state and external motion of the atoms is straightforward. For example, rate equations can be used (Allen and Eberly, 1975; Balykin and Letokhov 1987), or the Bloch equations (Allen and Eberly 1975), which can be extended to multi-level atoms and external motion (O'Kane *et al.* 1998). The addition of a second counter-propagating laser, as used in laser cooling or saturated absorption spectroscopy, creates a complex nonlinear system which is more difficult to solve (O'Kane *et al.* 1999) (see Section 4).
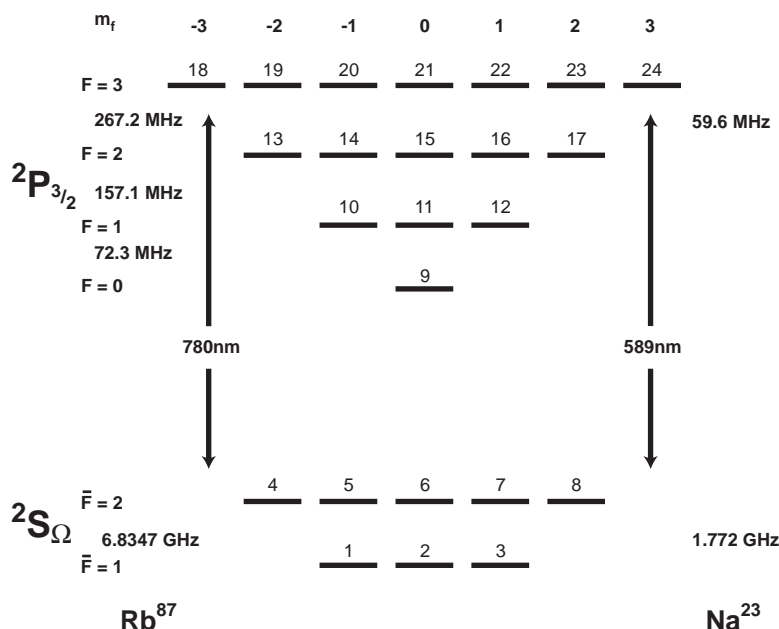
Fig. 2. Energy level diagram for the 24-level $5^2S_{1/2}$ and $5^2P_{2/3}$ states of Rb^{87} and the $3^2S_{1/2}, 3^2P_{3/2}$ states of Na^{23}. The energy splittings are shown for Rb^{87} on the left, and for Na^{23} on the right.

The alkali atoms are predominant in current atom optics research, due to their convenient optical transitions. Fig. 2 shows the relevant energy level structure of two important examples, rubidium (Rb^{87}) and sodium (Na^{23}). We describe an ensemble of such atoms, each with N internal states, by an $N \times N$ density matrix ρ whose diagonals represent the populations of the respective energy levels. The evolution of the density matrix elements is given by Liouiville's equation (Blum 1996)

$$i\hbar\frac{d\rho}{dt} = [H, \rho]\,, \tag{1}$$

where H is the Hamiltonian. To properly account for spontaneous decay of the atoms, the vacuum field must be included, so an appropriate Hamiltonian is

$$H = H_S + H_R + H_{SR}\,. \tag{2}$$

The three terms correspond to the atom+laser system, the vacuum reservoir, and the interaction between them. It is convenient to reduce the problem by explicitly including the expected spontaneous decay, leaving a modified density matrix which depends only on the atom+laser system Hamiltonian (see Section 5):

$$i\hbar\frac{d\rho_S}{dt} = [H_S, \rho_S] + \mathcal{L}_{\mathrm{relax}}[\rho_S]\,. \tag{3}$$

Here $\mathcal{L}_{\mathrm{relax}}[\rho_S]$ describes the decay of the excited state populations and off-diagonal coherences. This evolution equation is often referred to as the quantum master equation and, with appropriate Hamiltonian and relaxation terms, is equivalent to the optical Bloch equations (Allen and Eberly 1975).

The master equation can be solved numerically to calculate the time development of the internal state of the atoms, and hence to find the average force on the atoms and the atomic trajectory. Unfortunately, the large number of degrees of freedom make solution difficult, and approximations are required, particularly for real atoms with a rich internal structure. We first look at the very simplest approach, where we analytically derive a light-shift potential which drives the motion of the atoms, assuming a two-level atom, and then consider how the evolution of multi-level internal states can be included.

3. Two-level Semiclassical Method

In the two-level semiclassical method, we describe the light–atom interaction by a dipole potential which depends on the laser detuning, polarisation, and intensity. The detuning and polarisation are assumed fixed, and only the intensity varies. The atoms are taken to be point particles, with their motion controlled by the dipole force, that is, the gradient in the dipole potential. The potential is derived from a quantum treatment of the atom–laser interaction (Gordon and Ashkin, 1980), and the trajectories of the atoms are calculated using simple Newtonian mechanics (McClelland and Scheinfein 1991; McClelland 1995).

For a conservative potential we have

$$-m\ddot{x} = \frac{\partial U}{\partial x}\,, \tag{4}$$

where U is the potential, m the atomic mass, and $\ddot{x}$ the acceleration along axis x. The trajectory of the atom is then found using standard integration algorithms.

The primary advantage of this method lies in its speed and simplicity, and although in the first instance it treats the atoms as simple particles moving in the potential, it nevertheless yields information about the effect of a range of experimentally significant quantities such as the laser intensity and detuning, the temperature of the particles and the collimation of the beam. Newtonian modelling is thus an ideal candidate for testing experimental design and for tuning experimental parameters.

The dipole potential can be derived via a straightforward method based on Ehrenfest's theorem and the optical Bloch equations in the rotating wave approximation (Cook 1979; O'Kane et al. 1999; Cohen-Tannoudji 1990). We begin with the Hamiltonian for a two-level atom in a classical electromagnetic field,

$$H_S = \frac{p^2}{2m} + H_0 - \boldsymbol{\mu} \cdot \mathbf{E}(\mathbf{R}, t) \,, \tag{5}$$

where p is the atomic momentum, m is the mass, $\boldsymbol{\mu}$ is the atomic dipole moment operator and $\mathbf{E}(\mathbf{R}, t)$ is the electromagnetic field evaluated at the centre-of-mass position $\mathbf{R}$. In the Heisenberg representation, the operators $\mathbf{R}$ and $\mathbf{p}$ satisfy the equations of motion

$$\dot{\mathbf{R}} = \frac{\partial H}{\partial \mathbf{p}} = \frac{\mathbf{p}}{m},$$

$$\dot{\mathbf{p}} = m\ddot{\mathbf{R}} = \frac{-\partial H}{\partial \mathbf{R}} = \nabla \boldsymbol{\mu} \cdot \mathbf{E} \,. \tag{6}$$

Applying Ehrenfest's theorem gives

$$m\langle \ddot{\mathbf{R}} \rangle = \langle \nabla(\boldsymbol{\mu} \cdot \mathbf{E}) \rangle = \langle \boldsymbol{\mu} \nabla E \rangle \,. \tag{7}$$

Assuming ∇E is uniform across the wave packet (that is, provided the wave packet is small) the operator $\mathbf{R}$ can be replaced by its expectation value $\langle \mathbf{R} \rangle = \mathbf{r}$. We define our monochromatic field as $\mathbf{E} = \varepsilon_\nu E(\mathbf{r}(t), t)$ for constant polarisation ε_ν, where E can be described by

$$E(\mathbf{r}, t) = \tfrac{1}{2} E(\mathbf{r}) \left\{ \exp(i[\theta(\mathbf{r}) + \omega t]) + \exp(-i[\theta(\mathbf{r}) + \omega t]) \right\} \tag{8}$$

for frequency ω and phase θ. Here $\nu = 0$ for linear polarisation and $\nu = \pm 1$ for $\sigma_\pm$ circular polarisation.

Atomic motion is then determined by

$$\mathbf{F} = \langle \boldsymbol{\mu} \cdot \nabla E \rangle = \langle \boldsymbol{\mu} \cdot \varepsilon_\nu \rangle \nabla E (\mathbf{r}, t) \,, \tag{9}$$

where the expectation of the dipole moment is found from the density matrix:

$$\langle \boldsymbol{\mu} \cdot \varepsilon_\nu \rangle = \text{tr}(\rho \boldsymbol{\mu} \cdot \varepsilon_\nu) = \mu(\rho_{ge} + \rho_{eg}) \,. \tag{10}$$

Using the rotating wave approximation (Allen and Eberly 1975), we have

$$\langle \mu \cdot \varepsilon_\nu \rangle = \mu [\widetilde{\rho}_{ge} \exp i(\theta + \omega t) + \widetilde{\rho}_{eg} \exp -i(\theta + \omega t)] \,, \tag{11}$$

where $\widetilde{\rho}_{ge,eg}$ are the matrix elements in the rotating frame. Substituting this and equation (8) into (9) gives the equation of motion of the atom:

$$\mathbf{F} = m\frac{d^2\mathbf{r}}{dt^2} = \tfrac{1}{2}\mu\nabla E(\widetilde{\rho}_{ge} + \widetilde{\rho}_{eg}) - \frac{i}{2}\mu E\nabla\theta(\widetilde{\rho}_{ge} - \widetilde{\rho}_{eg}) \,. \tag{12}$$

The first term is the dipole force which we wish to use for atom focussing. The second term corresponds to the force felt by the atom due to spontaneous emission. This causes diffusion, but averages to zero and is ignored in this model.

It can be demonstrated that for most allowed atomic transitions, the electric dipole μ has time to reach the steady state before $\mathbf{r}$ has changed appreciably, and we can use the steady-state solutions (Cohen-Tannoudji 1990)

$$\widetilde{\rho}_{ge} + \widetilde{\rho}_{eg} = -\frac{2\Delta\Omega}{2\Omega^2 + 4\Delta^2 + \Gamma^2} \,. \tag{13}$$

Taking only situations of fixed σ^+ polarisation, the Rabi frequency is $\Omega = -\mu E/\hbar = \Gamma\sqrt{I_0/2I_{\text{sat}}}$ for an atomic decay rate of Γ, a travelling wave of intensity I_0, and a saturation intensity of $I_{\text{sat}} = \pi hc\Gamma/3\lambda^3$ where λ is the laser wavelength. The rate $\Gamma = 1/\tau$ is determined from the lifetime of the transition, $\tau = 16\cdot237\,\text{ns}$ for sodium (Oates *et al.* 1996) and $25\cdot8\,\text{ns}$ for rubidium (Belin 1971). The atoms have resonant frequency ω_0 and the laser detuning is $\Delta = (\omega - \omega_0)$. The equation of motion is then

$$\mathbf{F} = -\frac{\hbar\Delta\nabla(\Omega^2)}{2\Omega^2 + 4\Delta^2 + \Gamma^2} \,, \tag{14}$$

which defines a dipole potential U,

$$\mathbf{F} = -\nabla U \,, \tag{15}$$

where

$$U = \frac{\hbar\Delta}{2} \ln\left(1 + \frac{2\Omega^2}{4\Delta^2 + \Gamma^2}\right) \equiv \frac{\hbar\Delta}{2} \ln(1 + s) \,. \tag{16}$$

Here s is the saturation parameter, which can be written as

$$s = \frac{I}{I_{\text{sat}}} \frac{\Gamma^2}{(\Gamma^2 + 4\Delta^2)} \,. \tag{17}$$

We define

$$I = I(x, y, z) \equiv I_0 G(x, y, z) \,, \tag{18}$$

where $G(x, y, z)$ contains the spatial dependence of the laser field.

As an example, we first consider a simple lens for a beam of atoms. Several different lens systems have been suggested previously, including standing waves (McClelland *et al.* 1993; Timp *et al.* 1992; Drodofsky *et al.* 1997a, 1997b; McGowan *et al.* 1995), and TEM_{01}^{*} 'doughnut'-mode lasers. Doughnut-mode beams propagate similarly to standard Gaussian laser beams, but with a dark core. If the atomic and laser beams are coaxial, for blue detuning the atoms will be focussed towards the beam axis where the dark core minimises spontaneous decay and diffusion. This has not yet been demonstrated experimentally, perhaps because the coaxial arrangement is awkward. Focussing might also be achieved with transverse atomic and laser beams, by using a TEM_{01} laser. This mode propagates with a dark stripe between two bright back-to-back 'D'-shaped lobes (see Fig. 3). Atoms can be focussed into this dark region, and two orthogonal TEM_{01} laser beams then form a lens.
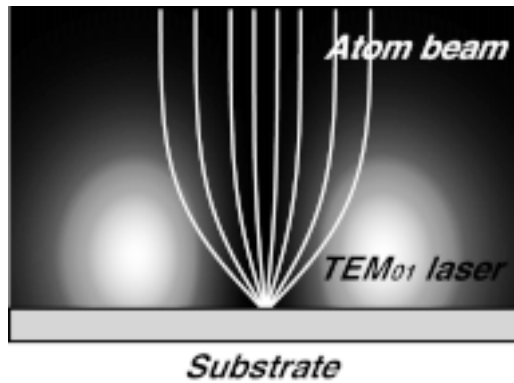
Fig. 3. Schematic of a TEM_{01} mode laser lens. The intensity profile for the laser beam is shown as though the beam is propagating across a substrate and out of the page. Atoms can be focussed into the dark region.

The transverse intensity profile for this lens is given by

$$G(x, y, z) = 8 \left[\frac{y^2}{\sigma_x^2} \exp\left(\frac{2(y^2 + z^2)}{\sigma_x^2} \right) + \frac{x^2}{\sigma_y^2} \exp\left(\frac{2(x^2 + z^2)}{\sigma_y^2} \right) \right], \qquad (19)$$

where $\sigma_{x,y}$ are the characteristic widths of the two beams. This intensity distribution yields a dipole potential of the form shown in Fig. 4.

Trajectories were calculated for atoms initially in a simple $20\,\mu$m square array of positions $300\,\mu$m above the surface. For each position, atoms were generated with a narrow range of angles and velocities. The velocities were weighted with a Maxwellian distribution, while the angular distribution of the atomic flux $F(a)$ in terms of angle a was of the form

$$F(a)da = \frac{V_{0z}^5}{(V_{0x}^2 + a^2 V_{0z}^2)^{\frac{5}{2}}}, \qquad (20)$$
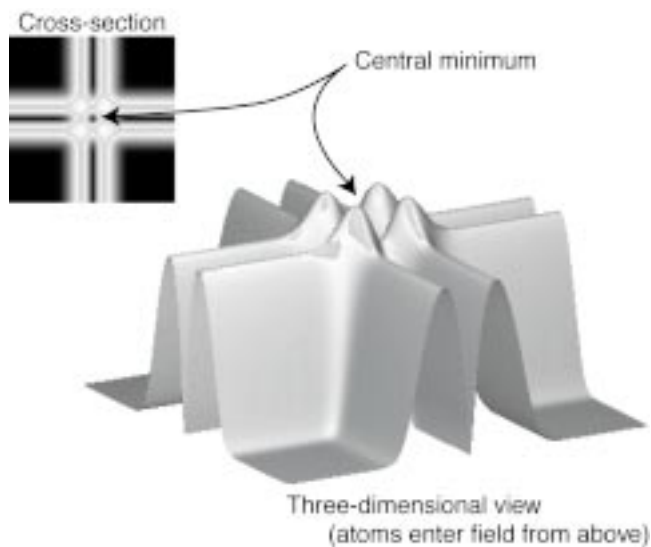
Fig. 4. Shaded surface representation of the dipole potential for two orthogonal TEM_{01} laser beams, together with (inset) a greyscale representation of a cross section through the plane of intersection of the two beams.

corresponding to a thermal source at temperature T with a longitudinal Maxwellian distribution defined by

$$V_{0z} = \sqrt{\frac{kT}{m}}, \qquad (21)$$

and where V_{0x} typically depends on the beam collimation defined by the experiment.
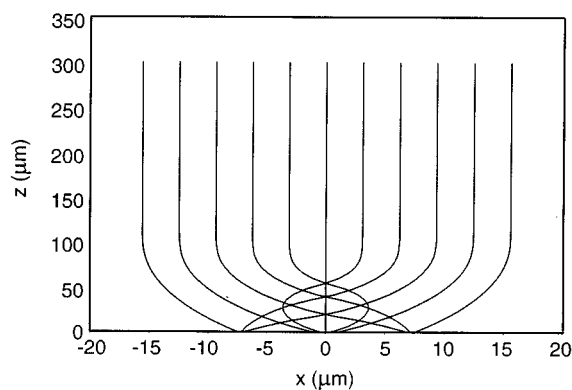
Fig. 5. Two-dimensional trajectories in a plane along the atomic beam axis for Rb^{87}. Longitudinal atomic velocity is $v = 17 \, \mathrm{m\,s^{-1}}$, peak laser intensity is $I_0 = 9 \cdot 0 \times 10^8 \, \mathrm{W\,m^{-2}}$, and the detuning is $200 \, \mathrm{MHz}$.
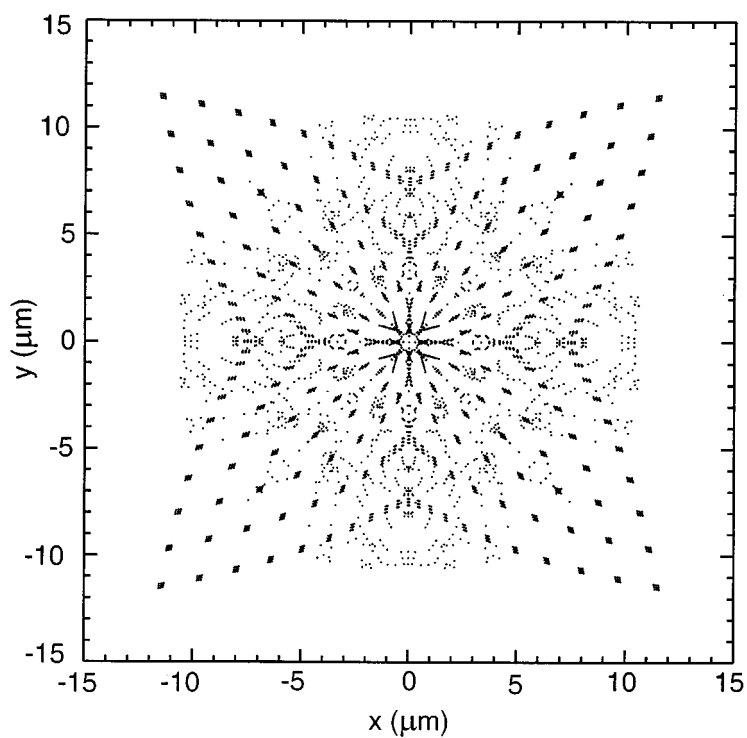
Fig. 6. Atomic distribution in the focal plane for Rb^{87} atoms focussed by a TEM_{01} lens. The atoms are initially spaced on a $20\,\mu m \times 20\,\mu m$ grid with $1\,\mu m$ spacing. Longitudinal atomic velocity is $v = 17\,\mathrm{m\,s^{-1}}$, peak laser intensity $I_0 = 9 \cdot 0 \times 10^8\,\mathrm{Wm^{-2}}$, and detuning $200\,\mathrm{MHz}$.
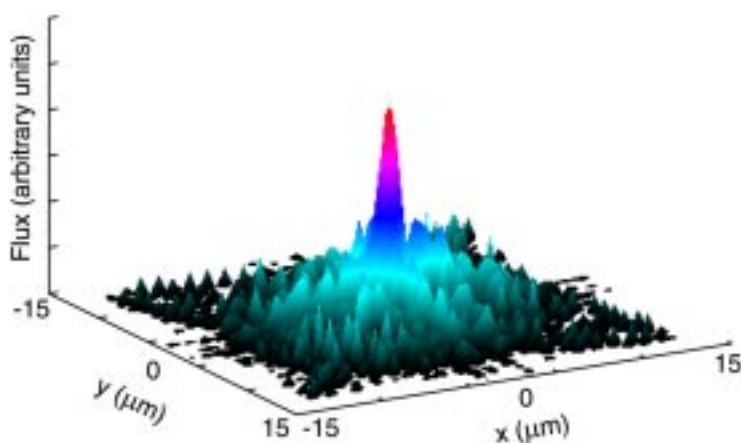
Fig. 7. Flux in the focal plane, weighted by the Maxwellian velocity distribution and angular distribution.

The trajectories of atoms travelling in a plane through the atomic beam axis are shown in Fig. 5. Fig. 6 shows the atomic distribution at the focal plane,

for a laser intensity of $I_0 = 9 \cdot 0 \times 10^8 \, \mathrm{W \, m^{-2}}$ detuned from atomic resonance by 200 MHz, an atomic beam temperature of 1 K corresponding to a maximum longitudinal velocity of $17 \, \mathrm{m \, s^{-1}}$, and a beam collimation of 1 mrad. The flux in the focal plane $z = 0$, appropriately weighted as described, is shown in Fig. 7 together with a profile through the centre in Fig. 8. A focal spot of about $3 \, \mu\mathrm{m}$ was achieved for these parameters.
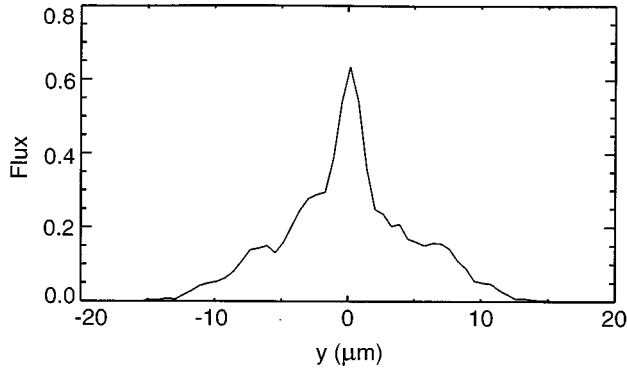

Fig. 8. Flux profile, showing a focal spot size of approx. $3 \, \mu\mathrm{m}$.

4. Optical Bloch Equations

The two-level semiclassical method is very fast numerically, but is only valid where the excited fraction is small, such that there is minimal spontaneous emission and consequent diffusion, and where the internal complexity of the atom can be ignored. These approximations are valid for far off-resonance detuning, but then the force is weak. We have developed an approach based on calculating the evolution of the internal state of the atom by solving the master equation written as a set of coupled differential equations, equivalent to the familiar two-level optical Bloch equations (OBE) but incorporating the full multi-level internal structure. They are solved using standard numerical integration techniques to provide the density matrix for the internal state of the atom, from which we find the force on the atom and hence the atomic trajectory.

The multi-level OBEs have been solved to calculate the internal state of atoms for travelling wave problems, in particular for laser-excited atomic collision studies (McClelland and Kelley 1985; Farrell *et al.* 1988). The simple addition of a counter-propagating laser beam, so as to create a standing wave, makes the solution much more difficult. However, atom interactions with a standing wave laser field are crucial to many problems, including gas lasers (Lamb 1964), saturation spectroscopy (Demtröder 1981) and laser cooling (Cohen-Tannoudji 1990; see also the special issue on Laser cooling and trapping of atoms 1989).

With two equal-intensity counter-propagating beams, the atoms move through a spatially-varying field, and therefore experience a time-dependent Hamiltonian. The strong nonlinearity of the atom–field coupling, even at the low intensities typical of saturated absorption spectroscopy, leads to sensitive dependence on the velocity, laser intensity, and atom trajectory. The evolution of the internal state and external motion of the atoms has been modelled using a broad

variety of techniques, including continued fractions (Stenholm and Lamb 1969), perturbation theory (Haroche and Hartmann 1972), rate equations (Nakayama 1997) and Monte Carlo wavefunction methods (Dalibard *et al.* 1992; Mölmer *et al.* 1993; Mölner 1994). These have provided valuable insight, but many of the important physical processes, in particular nonlinear effects, have been lost in the approximations.

We have developed a model for multi-level atoms, using optical pumping calculations for each individual atom as it moves through a true standing wave (O'Kane *et al.* 1999). This approach was used to accurately predict saturated absorption spectra for multi-level atoms, including the basic absorption peaks, power broadening, and merging of the hyperfine and cross-over resonances, in addition to a wealth of nonlinear phenomena that had not been predicted (O'Kane *et al.* 1999).
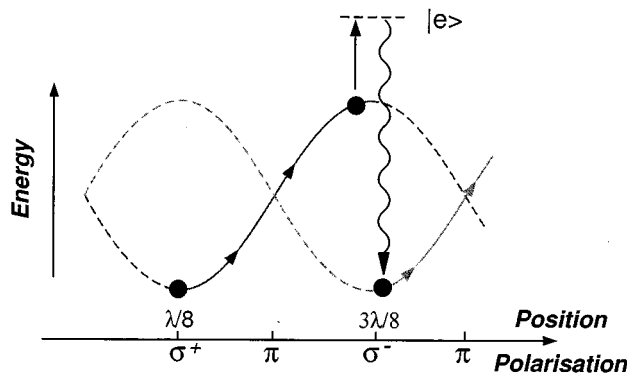
Fig. 9. Two counter-propagating linearly polarised laser beams, with orthogonal polarisations, produce a polarisation gradient field. This schematic indicates the dipole potential for two magnetic substates. Atoms moving along the polarisation gradient standing wave experience dipole potential gradients which can reduce their velocities.

Here we consider atoms in a laser-cooling arrangement (see Fig. 9), where we calculate the internal state of a sample of thermal atoms in a standing wave and show how cooling processes can then be simulated. Calculation of the atomic trajectories in a laser cooling configuration is a convenient test case, since laser cooling is well understood from analytic, experimental and Monte Carlo studies (Lett *et al.* 1989). Laser cooling of atomic beams is also essential to produce slow and collimated atomic beams which can then be focussed and patterned with a light field (Scholten *et al.* 1997).

We are particularly interested in (lin × lin) polarisation gradient cooling, where the two counter-propagating lasers are linearly polarised with orthogonal polarisation axes. This creates a field in which the polarisation varies along the beams, from circular to linear to reverse circular and so on. The field can be written as the sum of two circularly polarised beams with opposite helicities. The total field is given by $\mathbf{E}(z,t)$, with two components of real amplitude E_0 and respective polarisations $\varepsilon = \varepsilon_x$ and $\varepsilon' = \varepsilon_y$:

$$\mathbf{E}(z,t) = E^+(z)\exp(-i\omega_L t) + E^-(z)\exp(i\omega_L t)\,, \tag{22}$$

$$E^+(z) = E_0[\varepsilon\exp(ikz) + \varepsilon'\exp(-ikz)] \tag{23}$$

$$= E_0\sqrt{2}\left(\cos(kz)\frac{\varepsilon_x + \varepsilon_y}{\sqrt{2}} - i\sin(kz)\frac{\varepsilon_y - \varepsilon_x}{\sqrt{2}}\right)\,, \tag{24}$$

where $k = 2\pi/\lambda$.

We recall from our discussion of the two-level semiclassical model (equations 10 to 12) that we can derive the dipole force from consideration of the internal state. Hence we take for our Hamiltonian $H_S = H_0 + H_I$ where we have ignored the kinetic energy of the atom. The interaction term of equation (5), $H_I = -\boldsymbol{\mu}\cdot\mathbf{E}$, must be extended to multiple levels by summing over all ground-excited state pairs connected by the laser field; that is, using α and β to denote ground and excited states:

$$H_I = \sum H_{\alpha\beta}\,, \tag{25}$$

$$H_{\alpha\beta} = \sum_{\nu=\pm 1,0} C_{\alpha\beta}^{\nu}\left(-\boldsymbol{\mu}\cdot\mathbf{E}\right),$$

where $C_{\alpha\beta}^{\nu}$ is the Clebsch–Gordan coefficient for the $\alpha + \nu = \beta$ transition.

The time evolution of the density matrix elements is then given by equation (3) which expands to

$$\frac{d\rho_{\alpha\beta}}{dt} = -i\omega_{\alpha\beta}\ \rho_{\alpha\beta} - \frac{i}{\hbar}\sum_\gamma (H_{\alpha\gamma}\ \rho_{\gamma\beta} - \rho_{\alpha\gamma}\ H_{\gamma\beta}) + \mathcal{L}_{\mathrm{relax}}[\rho]\,. \tag{27}$$

The first term comes from the internal atomic energy H_0, and $\hbar\omega_{\alpha\beta}$ is the energy difference between states α and β.

In keeping with the usual derivation of the optical Bloch equations (Allen and Eberly 1975), we define the relaxation terms phenomenologically, but note that a rigorous derivation from QED first principles would include additional decay terms not considered here (Farrell *et al.* 1988). The decay terms are (Allen and Enerly 1975):

$$-\frac{1}{2\tau}\rho_{\alpha\beta}\ \text{for}\ \dot{\rho}_{\alpha\beta}\quad (\alpha \neq \beta)\,, \tag{28a}$$

$$-\frac{1}{\tau}\rho_{\beta\beta}\ \text{for}\ \dot{\rho}_{\beta\beta}\quad \text{(excited states)}\,, \tag{28b}$$

$$+\frac{1}{\tau}\sum_\beta \left(C_{\alpha\beta}^\nu\right)^2\ \text{for}\ \dot{\rho}_{\alpha\alpha}\quad \text{(ground states)}\,. \tag{28c}$$

For Rb^{87}, 24 internal states are involved (see Fig. 2). The time evolution equations with decay terms (equation 27) produce 576 coupled differential equations, with coefficients that have a cosinusoidal dependence on time due to the standing wave field (Cohen-Tannoudji 1990). We make several approximations to reduce the numerical task, firstly invoking the rotating wave approximation (Allen and Eberly 1975) and thereby eliminating all terms that oscillate at twice the optical frequency. We exclude all off-diagonal terms that do not couple an excited state to a ground state, and ignore coupling between magnetic sublevels of the same F level as well as off-diagonal pumping terms that couple from the $\overline{F} = 1$ ground state to the excited states. If the laser frequency ω_0 is tuned close to the $\overline{F} = 2$ transitions, then these terms will be significant only at very high velocities where the effective detuning brings them into resonance, or at very high laser intensities, where the power broadening causes significant overlap between the two hyperfine ground states. Finally, the density matrix is Hermitian (i.e. $\rho_{\alpha\beta} = \rho_{\alpha\beta}^*$) and so we are left with just 46 equations.

We first define the driving rate

$$\Omega_{ij} = \Omega \left(\varepsilon_{+1} \sin(kz) C_{ij}^{+1} + \varepsilon_{-1} \cos(kz) C_{ij}^{-1} \right) . \tag{29}$$

We then have the following sets of coupled equations:
$\overline{F} = 1$ ground state diagonals:

$$\frac{d\rho_{\alpha\alpha}}{dt} = \frac{1}{\tau} \sum_{\nu=0,\pm 1} \sum_{\beta=9}^{17} (C_{\alpha\beta}^{\nu})^2 \rho_{\beta\beta} . \tag{30}$$

$\overline{F} = 2$ ground state diagonals:

$$\frac{d\rho_{\alpha\alpha}}{dt} = -2\sqrt{2} \sum_{\beta=9}^{24} \Omega_{\alpha\beta} \operatorname{Im}(\widetilde{\rho}_{\alpha\beta}) + \frac{1}{\tau} \sum_{\nu=0,\pm 1} \sum_{\beta=9}^{24} (C_{\alpha\beta}^{\nu})^2 \rho_{\beta\beta} . \tag{31}$$

Excited state diagonals:

$$\frac{d\rho_{\beta\beta}}{dt} = 2\sqrt{2} \sum_{\alpha=4}^{8} \Omega_{\beta\alpha} \operatorname{Im}(\widetilde{\rho}_{\beta\alpha}) - \frac{1}{\tau} \rho_{\beta\beta} . \tag{32}$$
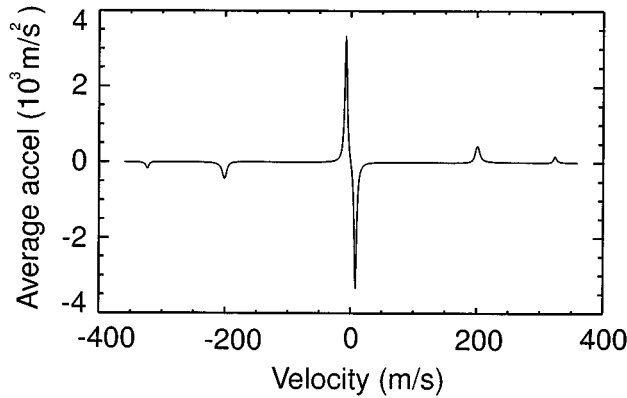
Off diagonals:

$$\frac{d\widetilde{\rho}_{\alpha\beta}}{dt} = i\sqrt{2}\Omega_{\alpha\beta} (\rho_{\alpha\alpha} - \rho_{\beta\beta}) + i(\omega_{\alpha\beta} - \omega_0)\widetilde{\rho}_{\alpha\beta} - \frac{1}{2\tau}\widetilde{\rho}_{\alpha\beta} . \tag{33}$$

We have solved these equations for a simple circularly polarised standing wave to calculate saturated absorption spectra for multi-level atoms (O'Kane *et al.* 1999). The density matrix was calculated for many random trajectories, corresponding to the Maxwellian distribution appropriate for a vapour cell absorption experiment, and averaged. This was repeated for a large number of laser detunings to produce an absorption spectrum. Excellent agreement with experimental saturated absorption spectra was obtained, including hyperfine and

cross-over resonances and saturation broadening. Thus the model accurately predicts the *internal* state of the atom, and we can apply the method to its external motion with some confidence.

Following the treatment of equations (10)–(12), we calculate the dipole force directly from the atomic density matrix and the field due to the laser:

$$\langle F(t)\rangle = -\sqrt{2}\hbar k\Omega \sum_{\alpha,\beta} \left(\cos(kz)C_{\alpha\beta}^{+1} + \sin(kz)C_{\alpha\beta}^{-1} \right) \mathrm{Re}(\widetilde{\rho}_{\alpha\beta}). \tag{34}$$


Fig. 10. Acceleration on Rb^{87} atoms as they are dragged through a one-dimensional polarisation gradient cooling standing wave at various velocities. The peak laser intensity is $I_0 = 1\cdot65$ mW cm^{-2} and the detuning is -10 MHz. Note the $F = 1, 2$ hyperfine resonances at about ±200 and ±300 m s^{-1}.

We can then solve the equations of motion for the atoms exactly as in Section 3, but now following the evolution of each atom's full multi-level internal state. Fig. 10 shows the average acceleration of a Rb^{87} atom as it is artificially dragged along the counter-propagating field at varying velocities. It maps out the dispersive force curve expected from a simple analytical two-level atom treatment (see Lett *et al.* 1989), but also shows additional force peaks due to other hyperfine levels. In Fig. 11 the force curve shows evidence of Dopplerons, a multi-photon effect due to absorption of photons from both laser components (Kyrölä and Stenholm 1977; Berman and Ziegler 1977). Finally, in Fig. 12 we plot the velocity of a single atom, initially travelling with a velocity of $0\cdot5$ m s^{-1} along the cooling lasers, as it is slowed and eventually trapped within a single potential well. Note that the density matrix approach gives an ensemble average for a 'single atom' calculation.

This technique is much more powerful than the two-level semiclassical method, since it includes the full multi-level internal structure of the atoms and multi-photon processes. Unfortunately, it is comparatively time consuming. The calculation in Fig. 12 required solution with the Runge–Kutta technique over approximately one million integration intervals for a single spatial dimension. Extension of the calculation to complex three-dimensional light fields is impractical, and we investigate Monte Carlo integration as an alternative which can also directly simulate diffusion.
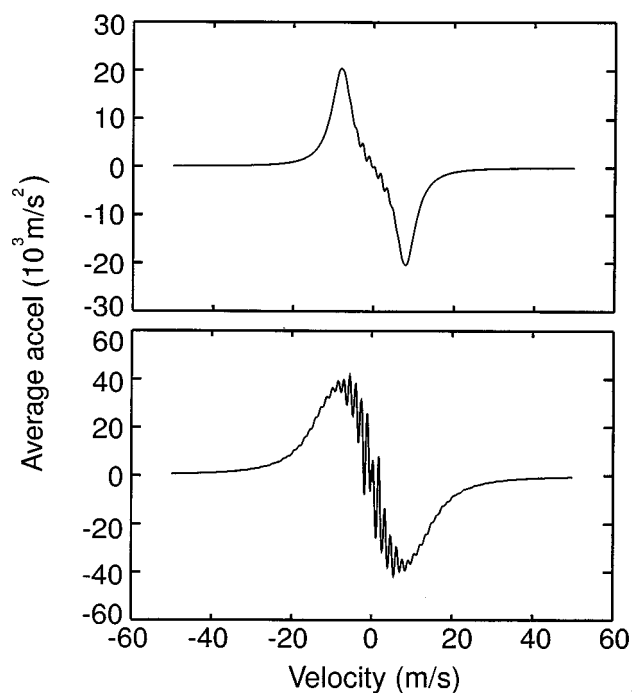
Fig. 11. Acceleration on Rb^{87} atoms as they are dragged through a one-dimensional polarisation gradient cooling standing wave at various velocities. The detuning is -10 MHz, and the peak laser intensity is $I_0 = 16 \cdot 5$ mW cm^{-2} (top) and $I_0 = 165$ mW cm^{-2} (bottom). Note the 'Doppleron' resonances.
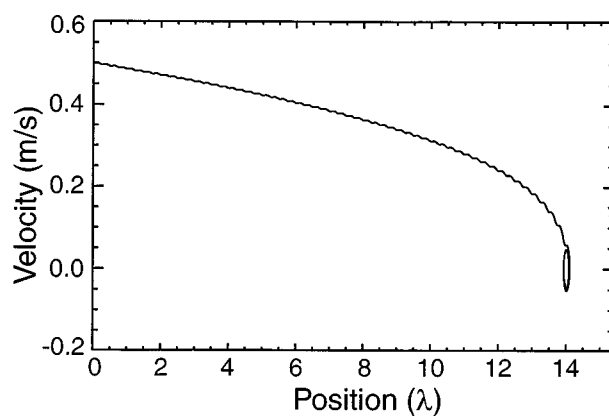
Fig. 12. Atomic trajectory for one-dimensional polarisation gradient cooling of a Rb^{87} atom. The velocity along the cooling laser beam axis is shown as the atom begins at position $z = 0$ and velocity $v = 0 \cdot 5$ m s^{-1} and slows as it travels through the cooling region, eventually becoming trapped in a single potential well at $z \approx 15 \, \mu$m.

5. Monte Carlo Wavefunction Method

The optical Bloch method has several significant limitations. It is semiclassical in that it treats the atoms as point particles, which is inappropriate at the low temperatures that can be achieved with laser cooling. It is inherently averaging, calculating the density matrix for an ensemble of atoms for a given laser field and atomic velocity. Spontaneous decay effects, in particular recoil of the atom, are averaged to zero, and hence diffusion is not calculated. In addition, when calculating the internal density matrix, symmetries reduce the integration task (e.g. from 576 to just 46 equations for Rb^{87}), but a similar reduction is generally not possible for momentum states added to describe the external motion. A large set of states is required to adequately describe the motion in three dimensions, and the computation time becomes exorbitant.

The Monte Carlo wavefunction method (MCWF), developed for laser cooling by Dalibard *et al.* (1992), can provide improved integration times, implicitly treats the atoms as wavepackets, and directly shows the effects of diffusion. Instead of calculating an ensemble average, the MCWF calculates what might happen to an individual atom, and averages over many such atoms.

Here we use the MCWF method for optical pumping calculations, i.e. to calculate the evolution of the internal state of the atoms, and compare the results with those obtained from the Bloch method. The MCWF treatment does not provide any advantages if only the internal state is required. Nevertheless, the internal state must be calculated before attempting to calculate trajectories, and the results also provide a useful test to ensure proper implementation of the formalism.

The essence of the method is based on the repetition of two simple processes. Firstly we evolve the atomic wavefunction using an approximate (non-hermitian) Hamiltonian, for a short time dt. Then we randomly decide whether the atom spontaneously decays, in which case we collapse the atomic state back to the ground state; if not, we renormalise the wavefunction. Of course, the random collapse must occur with a probability such that the atom decays at the proper transition rate.

(5a) Two-level Monte Carlo

It is very useful to first consider the two-level model, which includes all the essential elements of the MCWF method, and then add the additional terms for treating multi-level atoms. The formalism of the two-level problem is well described, for example by Dum *et al.* (1992), in the lecture notes of Mölmer (1994), and more recently by Mölmer and Castin (1996).

The problem is the same as that of the OBE treatment: we wish to solve the master equation (equation 3)

$$i\hbar\frac{d\rho_S}{dt} = [H_S, \rho_S] + \mathcal{L}_{\text{relax}}[\rho_S],\qquad(35)$$

where, in the rotating wave approximation, the two-level system Hamiltonian H_S is given by (Dum *et al.* 1992)

$$H_S = \frac{\hbar}{2}\Delta(|g\rangle\langle g| - |e\rangle\langle e|) - \frac{\hbar\Omega}{2}(|e\rangle\langle g| + |g\rangle\langle e|)\qquad(36)$$

and the relaxation terms are

$$\mathcal{L}_{\text{relax}}[\rho_S] = -\frac{\Gamma}{2}\left\{|e\rangle\langle e|\rho_S + \rho_S|e\rangle\langle e|\right\} + \Gamma|g\rangle\langle e|\rho_S|e\rangle\langle g|\,. \tag{37}$$

The relaxation terms describe decay from the excited state population at rate Γ, decay of the coherences ρ_{ge} and ρ_{eg} at rate $\Gamma/2$, and an increase in the population of the ground state at rate Γ.

In the Monte Carlo approach, instead of calculating the evolution of the full density matrix, we instead evolve the system wavefunction from some initial state, i.e.

$$|\psi(0)\rangle = c_g(0)|g\rangle + c_e(0)|e\rangle\,, \tag{38}$$

and we keep only the wavefunction amplitudes without coherences. We introduce an *effective* Hamiltonian which adds decay from the excited state population that mimics some of the relaxation effects:

$$H_S \to H_{\text{eff}} \equiv H_S - \frac{i\hbar\Gamma}{2}|e\rangle\langle e|\,. \tag{39}$$

Note that H_{eff} is non-hermitian: while it reduces the excited state amplitude, it also reduces the total norm of the wavefunction.

Starting with the initial state, the wavefunction amplitudes (in this case a two-component vector representing c_g and c_e) are propagated in time for small time increments δt, where δt should be smaller than any time scale of physical significance, i.e. $\delta t \ll \Gamma^{-1}, \Omega^{-1}, \Delta^{-1}$. After each time step, we decide randomly (but weighted according to the known atomic lifetime) if the system should collapse to the ground state $|g\rangle$. We approximate the Heisenberg evolution to first order:

$$\left|\psi^{(1)}(t+\delta t)\right\rangle = \left(1 - \frac{iH_{\text{eff}}}{\hbar}\delta t\right)|\psi(t)\rangle\,, \tag{40}$$

where $\langle\psi^{(1)}(t+\delta t)\mid\psi^{(1)}(t+\delta t)\rangle = 1 - \delta p$, and the jump probability δp is determined by the atomic lifetime and the excited state population:

$$\delta p = \Gamma|c_e|^2\delta t\,. \tag{41}$$

This probability is compared to a random number $\epsilon \in [0,1]$ and if $\epsilon < \delta p$ the collapse occurs, otherwise the state function $|\psi(t+\delta t)\rangle$ is renormalised because the approximation equation (40) is non-Hermitian.

Fig. 13 shows the excited state population $|c_e|^2$ as it evolves in time, showing absorption and the beginnings of stimulated emission broken by collapse to the ground state through spontaneous decay. Calculating many such evolutions and averaging, we find the expected ensemble average which might be measured experimentally, as shown for 10 000 atoms in Fig. 14 (see also Dum *et al.* 1992).
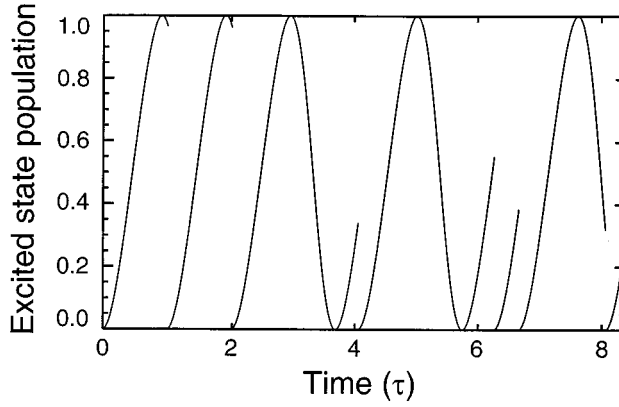
Fig. 13. Monte Carlo wavefunction results for the excited state population in a two-level atom. The laser is σ^+ circularly polarised, with intensity such that the Rabi frequency is $\Omega = 3\Gamma$, with zero detuning.
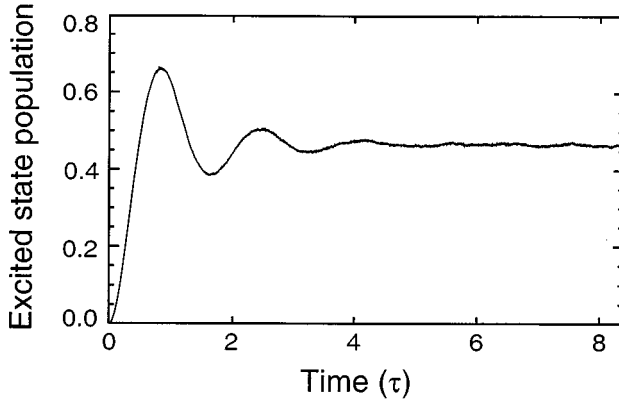
Fig. 14. Two-level MCWF results averaged for 10 000 atoms. The expected Rabi oscillation damping and steady-state population are observed.
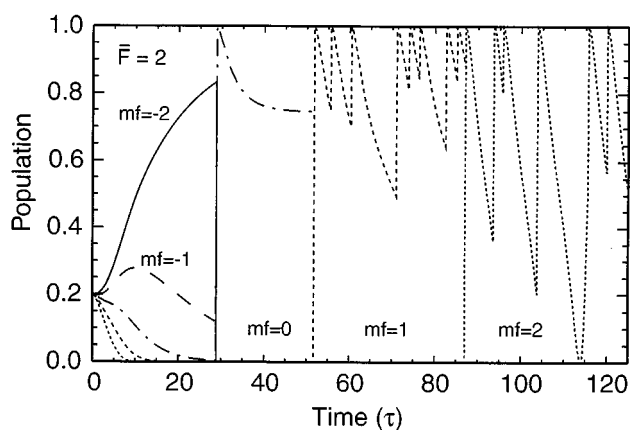
(5b) Multi-level Monte Carlo

Extension of the MCWF method to multi-level atoms is straightforward. The effective Hamiltonian of equation (39) is modified to include all allowed decay channels:

$$H_{\text{eff}} \equiv H_S - \frac{i\hbar}{2} \sum_{\alpha,\beta} |\alpha\rangle\langle\beta| \,. \tag{42}$$

In evaluating the jump probabilities (equation 41), δp must now be summed over all possible decays, i.e.

$$\delta p = \sum_i \delta p_i \,, \tag{43}$$

Fig. 15. Monte Carlo wavefunction results for the $\overline{F} = 2$ magnetic substate populations of a 17-state $\overline{F} = 2 \rightarrow F = 2, 3$ sodium atom. The atomic state is initially set to a superposition of all five ground states. The atom is progressively pumped to the $m_f = +2$ substate, but note that at 30 lifetimes, the atom collapses to the $m_f = 0$ substate, skipping the $m_f = -1$ substate.
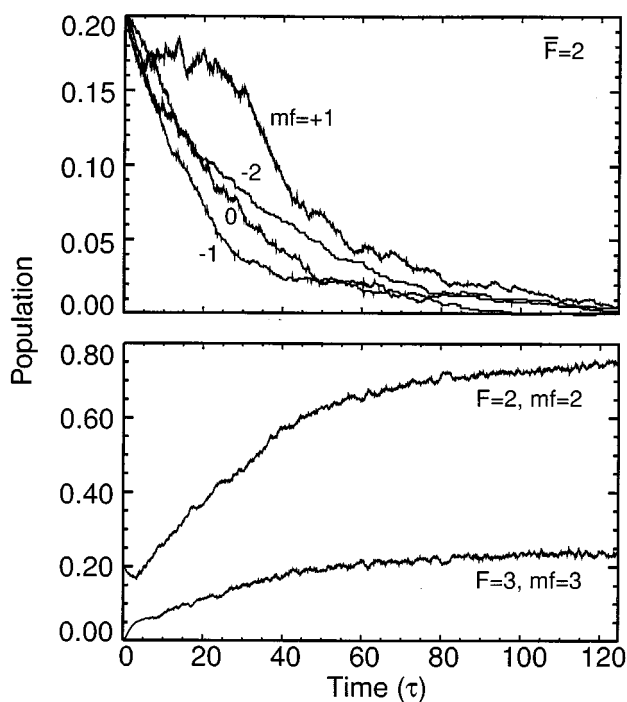

Fig. 16. Three-level MCWF results for ground states (top) and excited states (bottom), for a peak laser intensity of $I_0 = 6$ mW cm^{-2}, averaged for 1000 atoms. The behaviour is as expected, but significant noise is apparent.

$$\delta p_i = \delta t \langle \psi(t)|(C_{\alpha\beta}^{\nu})^2|\psi(t)\rangle\,, \tag{44}$$

where i describes all the allowed $\alpha + \nu = \beta$ decay transitions. If the jump occurs, then the final collapsed state will be decided by comparing a second random number to the relative probabilities $\delta p_i/\delta p$.

We have applied this method to 17-level Na^{23}, including only the $\overline{F} = 2$ and $F = 2, 3$ hyperfine levels. Fig. 15 shows the evolution of a single atom, and Fig. 16 shows the average of 1000 atoms. We have also used the optical Bloch equations (as detailed in McClelland and Kelley 1985), and quantitative agreement is obtained for 10 000 atoms, as shown in Fig. 17.
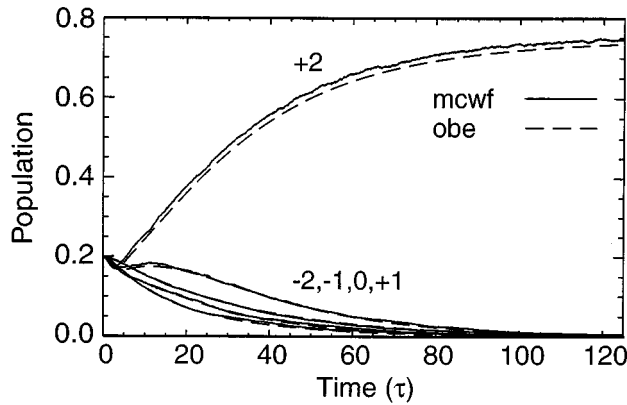
Fig. 17. Comparison of results from MCWF and optical Bloch methods, for optical pumping of the 17-level sodium system, showing quantitative agreement. The MCWF results are an average of 10 000 atoms.

The MCWF results for 10 000 atoms required approximately 400 times longer than the equivalent Bloch equation solution, and so the Bloch method is clearly preferable for optical pumping calculations. It is important to note however that the inclusion of external momentum states results in a product wavefunction $|\alpha\, m_\alpha\, p\rangle$, where α denotes both ground and excited states, m_α the magnetic substructure and $|p\rangle$ the momentum eigenfunctions for atomic motion in the direction of laser propagation. Solving these requires a large number of differential equations. For example a basis set of 40 momentum states coupled with a minimal 12 internal (5 ground, 7 excited) basis states, for the $\overline{F} = 2 \rightarrow F = 3$ transition in sodium, results in a set of 360 coupled differential equations using MCWF, and $360^2 = 129\,600$ for the OBEs. The latter can be reduced somewhat as described above, using internal symmetries, but the number will remain large.

A similar system was considered by Hoogerland *et al.* (1990) where the MCWF method was applied to the calculation of photon statistics and resonance fluorescence in a supersonic beam of metastable neon ($\overline{J} = 2 \rightarrow J = 3$). In a calculation of the final momentum distributions of the wavefunctions good agreement with experiment was found after only 1000 realisations, an order of magnitude reduction compared to that needed for the associated optical pumping

calculation (see Fig. 17). Thus for calculating external motion, the Monte Carlo method is well worth pursuing.

6. Summary and Conclusions

The development of atom optical devices is of considerable interest to a large component of the physics community. Even simple devices such as lenses offer challenging problems, and realistic calculation of their behaviour is essential before committing to experimental verification. We have pursued several alternate techniques, including two-level and multi-level semiclassical trajectory calculations and Monte Carlo simulations.

The two-level semiclassical approach is intuitive and fast, allowing rapid testing of ideas. However, it neglects changes in the internal state of the atom, assuming minimal excitation. It also provides no measure of the important diffusion processes, and will not predict any effects due to atomic interference. The multi-level density matrix formalism fully accounts for the dynamics due to the evolution of the internal state of the atom, at some cost in terms of computation time. The semiclassical models neither incorporate the de Broglie wave nature of the atoms nor include diffusion, although the latter might be incorporated (Berg-Sörensen *et al.* 1992; Ungar *et al.* 1989 Nienhuis *et al.* 1991). The Monte Carlo wavefunction method allows realistic prediction of all these physical effects, but at considerable cost computationally.

The appropriate model for any given problem in laser–atom interactions depends on the outcomes sought. For many questions facing us in our exploration of atom optical systems, the two-level semiclassical method is very valuable, but the multi-level Bloch equations and Monte Carlo methods have provided us with rich insight into the complexity of the laser–atom system.

Acknowledgments

References

Adams, C. S., Sigel, M., and Mlynek, J. (1994). *Phys. Rep.* **240**, 143.
Allen, L., and Eberly, J. H. (1975). 'Optical Resonance and Two-level Atoms' (Wiley: New York).
Balykin, V. I., and Letokhov, V. S. (1987). *Opt. Commun.* **64**, 151.
Belin, G. (1971). *Phys. Scripta* A **4**, 269.
Berg-Sörensen, K., Castin, Y., Bonderup, E., and Mölmer, K. (1992). *J. Phys.* B **25**, 4195.
Berman, P. R., and Ziegler, J. (1977). *Phys. Rev.* A **15**, 2042.
Blum, K. (1996). 'Density Matrix Theory and Applications' 2nd edn (Plenum: New York).
Celotta, R. J., Gupta, R., Scholten, R. E., and McClelland, J. J. (1996). *J. Appl. Phys.* **79**, 6079.
Cohen-Tannoudji, C. (1990). *In* 'Fundamental Systems in Quantum Optics', pp. 1–161 (Les Houches).
Cook, R. J. (1979). *Phys. Rev.* A **20**, 224.
Dalibard, J., Castin, Y., and Mölmer, K. (1992). *Phys. Rev. Lett.* **68**, 580.
Demtröder, W. (1981). 'Laser Spectroscopy', 2nd edn (Springer: Berlin).
Drodofsky, U., Stuhler, J., Schulze, T., Drewsen, M., Brezger, B., Pfau, T., and Mlynek, J. (1997*a*). *Appl. Phys.* B **65**, 755.

Drodofsky, U., Stuhler, J., Schulze, T., Drewsen, M., Brezger, B., Pfau, T., and Mlynek, J. (1997*b*). *Microelect. Engineering* **35**, 285.

Dum, R., Zoller, P., and Ritsch, H. (1992). *Phys. Rev. A* **45**, 4879.

Farrell, P. M., MacGillivray, W. R., and Standage, M. C. (1988). *Phys. Rev. A* **37**, 4240.

Gordon, J. P., and Ashkin, A. (1980). *Phys. Rev. A* **21**, 1606.

Gupta, R., McClelland, J. J., Jabbour, Z. J., and Celotta, R. J. (1995). *Appl. Phys. Lett.* **67**, 1378.

Haroche, S., and Hartmann, F. (1972). *Phys. Rev. A* **6**, 1280.

Hoogerland, M. D., Wijnands, M. N. J. H., Senhorst, H. A. J., Heijerinck, H. C. W., and van Leeuwen, K. A. H. (1990). *Phys. Rev. Lett.* **65**, 1559.

Kyrölä, E., and Stenholm, S. (1977). *Opt. Commun.* **22**, 123.

Lamb, W. E., Jr (1964). *Phys. Rev. A* **134**, A1429.

Laser cooling and trapping of atoms (1989). *Special issue, J. Opt. Soc. Am.* **6**, 2020–226.

Lett, P. D., Phillips, W. D., Rolston, S. L., Tanner, C. E., Watts, R. N., and Westbrook, C. I. (1989). *J. Opt. Soc. Am. B* **6**, 2084.

McClelland, J. J. (1995). *J. Opt. Soc. Am. B* **12**, 1761.

McClelland, J. J., and Kelley, M. H. (1985). *Phys. Rev. A* **31**, 3704.

McClelland, J. J., and Scheinfein, M. R. (1991). *J. Opt. Soc. Am. B* **8**, 1974.

McClelland, J. J., Gupta, R., Jabbour, Z. J., and Celotta, R. J. (1996). *Aust. J. Phys.* **49**, 555.

McClelland, J. J., Scholten, R. E., Palm, E. C., and Celotta, R. J. (1993). *Science* **262**, 877.

McGowan, R. W., Giltner, D. M., and Lee, S. A. (1995). *Opt. Lett.* **20**, 2525.

Mölmer, K. (1994). 'Lectures at the Winter School on Quantum Optics' (ICTP: Trieste, Italy).

Mölmer, K., and Castin, Y. (1996). *Quant. Semiclass. Opt.* **8**, 49–72.

Mölmer, K., Castin, Y., and Dalibard, J. (1993). *J. Opt. Soc. Am. B* **10**, 524.

Nakayama, S. (1997). *Phys. Scripta* T **70**, 64.

Nienhuis, G., van der Straten, P., and Shang, S.-Q. (1991). *Phys. Rev. A* **44**, 462.

Oates, C. W., Vogel, K. R., and Hall, J. L. (1996). *Phys. Rev. Lett.* **76**, 2866.

O'Kane, T. J., Scholten, R. E., Farrell, P. M., and Walkiewicz, M. R. (1999) *Phys. Rev. A* **59**, 4485.

Scholten, R. E., Gupta, R., McClelland, J. J., Celotta, R. J., Levenson, M. S., and Vangel, M. G. (1997). *Phys. Rev. A* **55**, 1331–8.

Scholten, R. E., McClelland, J. J., Palm, E. C., Gavrin, A., and Celotta, R. J. (1994). *J. Vac. Sci. Tech. B* **12**, 1847.

Stenholm, S., and Lamb, W. E., Jr (1969). *Phys. Rev.* **181**, 618.

Timp, G., Behringer, R. E., Tennant, D. M., Cunningham, J. E., Prentiss, M., and Berggren, K. K. (1992). *Phys. Rev. Lett.* **69**, 1636.

Ungar, P. J., Weiss, D. S., Riis, E., and Chu, S. (1989). *J. Opt. Soc. Am. B* **6**, 2058.